# SS and *LCC–LCC* in Simultaneous Wireless Power and Data Transfer: A Comparative Analysis for SAE J2954-Compliant EVs

Inmaculada Casaucao , Alicia Triviño , Fabio Corti , *Member, IEEE*,
and Alberto Reatti , *Member, IEEE*

*Abstract*—**Simultaneous wireless power and data transfer (SWPDT) is a technology that enables the transfer of electrical power and data signals at the same time. Since the transfer is performed through the same physical link, particular attention must be placed on the frequency response and mutual influence between data and power channels. Although several studies have been proposed for SWPDT modeling applied to electric vehicles (EV), an extensive analysis of the influence of misalignment on the frequency response of the data channels is lacking in the literature. This article investigates the robustness to misalignment of the data channel using two main resonant topologies, such as those based on series–series (SS) and *LCC–LCC* compensation circuits. The analytical model of the data channel is derived for both topologies and the performances are evaluated in two lab prototypes using the misalignment scenarios described in the SAE J2954 standard. Variables, such as efficiency, signal-to-noise ratio (SNR), and capacity of the data channel have been analyzed. Similarly, attention has been paid to backward data transmission, which is of interest for vehicle-to-grid chargers. The obtained results in each analysis show that the data channel in *LCC–LCC* topology has a more stable and symmetrical performance.**

*Index Terms*—**Bandwidth, data transfer, electric vehicle (EV), gain, *LCC*, misalignment, signal-to-noise ratio (SNR), series–series (SS), simultaneous wireless power and data transfer (SWPDT).**

## I. INTRODUCTION

WIRELESS charging of electric vehicle (EV) introduces new advantages over wired charging, as the driver's involvement in the charging process is minimized. An inductive WPT system consists of a primary circuit (transmitter) and secondary circuit (receiver), as shown in Fig. 1. A pair of air-core coupled coils is used for power transmission. For EV charging, the primary circuit is located in the electric vehicle supply equipment (EVSE), and the secondary circuit in the EV. It is important to note that a compensation mechanism on both sides is required in an inductive-resonant wireless power transfer system, allowing the system to work in resonance at a given frequency. Hence, these structures enhance and improve power transmission [1]. In the literature, there are two notable compensation systems with similar characteristics used for EV SWPDT systems: series–series (SS) and *LCC–LCC* [2]. The SS compensation system is one of the most widespread and widely used, because of its simplicity, its design is independent of the load, it has more stable behavior faced with the bifurcation phenomenon, and needs for a smaller amount of copper in the windings [3]. The *LCC–LCC* compensation systems (named in the rest of this article as *LCC*) result in an output current independent of the load, filter a large proportion of the harmonics found at the inverter and rectifier output, allow for a zero-voltage switching (ZVS), and have great deal of freedom in design [4]. Both topologies show a good performance in the misalignment phenomenon for power transfer, which is required in conventional EV wireless charging.

In the charging process of an EV, information is exchanged between the EVSE and the EV through the charging connector. This requires a wireless information transmission system to be included in the system. Commercial technologies can be used, such as bluetooth, bluetooth low energy, Zig-Bee, radio frequency, and IEEE 802.11 (Wi-Fi) for this application, but all of them have some drawbacks, such as pairing problems, connection losses, transmission delays, and cybersecurity issues, which are a crucial aspect [5]. Cyberattacks compromise private user information, such as account numbers or personal data, or they could cause physical damage to the infrastructure and/or EV with incorrect charging. A possible solution is the replacement of commercial technologies with power circuits, which allows for data transmission. This double circuit is named simultaneous
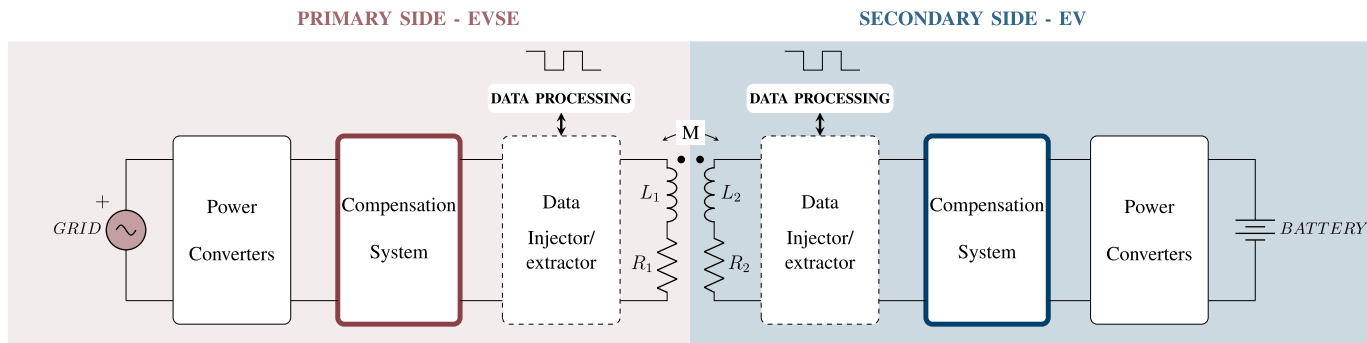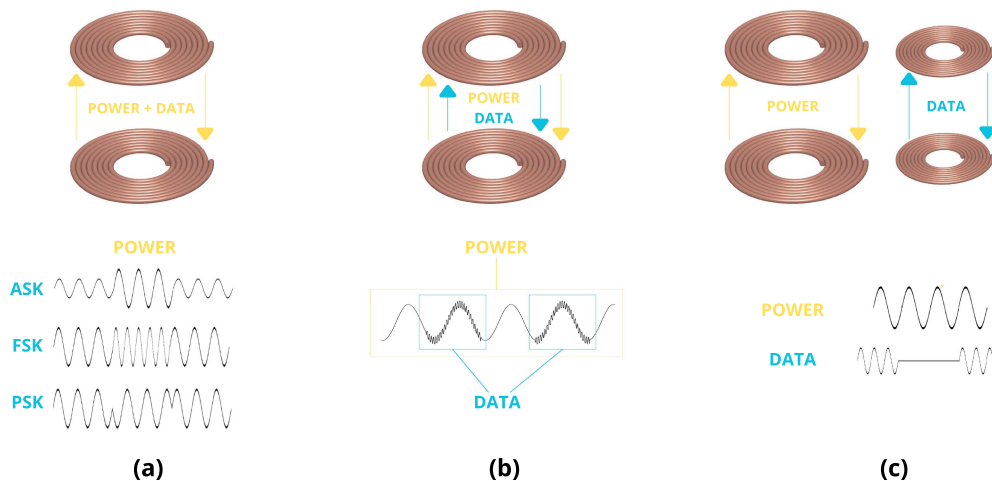
Fig. 1.    Generic SL-DC SWPDT system.



Fig. 2.    SWPDT topologies. (a) SL-SC. (b) SL-DC. (c) DL-DC.

wireless power and data transfer (SWPDT) systems, and numerous designs are available in the literature, as indicated in [6].

These technologies are mainly classified as single link-single carrier (SL-SC), double link-double carrier (DL-DC), and single link-double carrier (SL-DC) [7], as shown in Fig. 2. In SL-SC, the data transmission is accomplished through the modification of the power signal, either in frequency, amplitude, or phase. These modifications are detected in the data receiver circuit and demodulated for interpretation. All the transmission takes place through a single pair of coupled coils, affecting the data transfer to the power transmission. In contrast, in a DL-DC system power and data are transmitted at the same time through different channels, by using two completely independent signals and, at least, two pairs of coupled coils. Finally, in SL-DC topology two different signals are used, one for power and one for data, transmitted through a single pair of coupled coils. In this case, the frequencies used for each of these signals must be at least one order of magnitude apart. Thus, if the power signal is transmitted on a carrier of the order of kHz, it is recommended that the data signal be of the order of MHz. SL-DC is one of the most versatile and extensively used systems, able to combine the benefits of the other configurations. In an SL-DC system the characteristics offered by this particular data channel must be carefully investigated to determine whether variables, such as bandwidth or bit-rate are suitable for the communication requirements. Initially, the characteristics are expected to vary under coil misalignments. Communication and power circuit in SL-DC systems share some electronic elements and, therefore, the power components may affect the communication performance.

The role of compensation systems is crucial as they are reactive elements, which have different impedance and performances also depending on the operating frequency. This is why in SL-DC systems, it is recommended to keep the frequency of the data signal at least one order of magnitude higher than the frequency of the power signal.

The study of transfer functions is fundamental to the development of an SWPDT system, in order to understand the performance that the communication system can offer. The authors in [8] and [9] studied the transfer functions of an *LCC* compensation system, while in [10] and [11], the studied topology is SS. No misalignment study has been found in these cited papers. However, these papers do not consider the parasitic resistances of all the reactive component, which have relevant effects on EV wireless charging. Yao et al. [12] included a brief analysis of the misalignment effects, they indicate that the

system they propose remains essentially unaffected at different misalignment distances. This analysis is carried out with generic distances, without distinguishing between the possible misalignment axes. In contrast, Wang et al. [13] showed a graph where the data channel gain increases with the mutual inductance $M$, without phase analysis. The reviewed literature also includes comparisons of both compensation systems in terms of power channel [14], [15]. To the best of authors' knowledge, no comparative study has been carried out to analyze the performance of these two main technologies in terms of data transmission. In particular, it is useful for the designers to investigate how the data transfer performs when there is a coil misalignment, which is a typical operation of EV wireless charger [16]. In fact, SAE J2954 establishes that misalignment could occur in three axes ($X$, $Y$, $Z$) and sets maximum conditions for each of them. It is noteworthy the importance of the analysis of the transfer functions not only in terms of gain, but also in phase, as it influences some modulation techniques, such as PSK.

In this article, the performance of the SS and *LCC* compensation topologies in an SL-DC system, is analyzed not only considering the power transmission but also including data transmission. The significance and the novelty of this article is that the parasitic resistances of all reactive elements have been considered. Furthermore, the integration of the SWPDT system for a real EV charger prototype, whose dimensions and parameters are determined by the SAE J2945 standard has been carried out.

The main contributions of this article are as follows.

1) The definition of the transfer function (in terms of gain and phase) for the data and power channels in an SWPDT EV charger. The formulation includes the parasitic resistances of reactive components, which have a significant impact on the system performance as we have demonstrated for SS and an *LCC* compensation systems. To validate the transfer functions under realistic conditions, we have considered the variation of the parasitic resistance with the working frequency as two frequencies are involved in these EV applications.

2) The theoretical analysis of the bandwidth offered by the data channel for both compensation systems to understand the effects of typical coil misalignment conditions identified by SAE J2954.

3) The study of the impact of the data channel on the power channel and vice versa for the conditions set in SAE J2954. For this purpose, it has been analyzed the signal-to-noise ratio (SNR) between the power and data signals and the capacity (bits/s) for each misalignment distance and at different power levels, studying the trend of the curves under variations of the input voltage.

4) The study of the backward data transmission, with a comparative between forward and backward performance for both topologies. The study of backward transmission is of interest for the integration of wireless EV chargers with vehicle-to-grid (V2G) control systems. In this context, communication occurs in both directions, and the performance for each compensation topology is different.
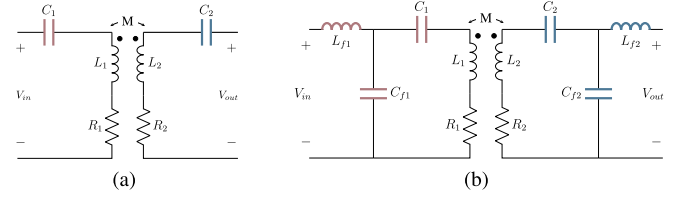


Fig. 3. Basic structures of (a) SS compensation system, (b) *LCC* compensation system.

5) The design and experimental tests of SS and *LCC* prototypes to validate the theoretical approach.

The rest of this article is organized as follows. Section II gives a basic description of the SS and *LCC* systems designs. In Section III, an analytical study of transfer functions for power and data channel is carried out, both for SS and *LCC* compensation systems. The experimental validation of the previous analytical study is described in Section IV. In Section V, a theoretical and experimental analysis of misalignment conditions in SS and *LCC* configurations is performed. Finally, Section VI concludes this article.

## II. DESIGN OF THE COMPENSATION TOPOLOGIES

Compensation circuits are typically installed in EV wireless chargers to make the system operate at resonance and improve the power transmission. In this article, the design and implementation of SS and *LCC* compensation systems has been carried out, as shown in Fig. 3.

The capacitors used for the SS compensation system are calculated according to

$$C_i|_{i=\{1,2\}} = \frac{1}{\omega_p^2 L_i} \tag{1}$$

where $\omega_p = 2\pi f_p$, and $f_p$ is the power channel frequency.

For *LCC* compensation system two different parameters must be considered: capacitor values and extra added coils values. Extra coils ($L_{f1}$ and $L_{f2}$) are sized assuming that the inductance value is at least the value of the coupling coefficient of the system, so that $[L_{f1}, L_{f2}] > M$, as suggested in [18]. The capacitor value is given by

$$C_i|_{i=\{1,2\}} = \frac{1}{\omega_p^2 (L_i - L_{fi} + T_{nX})} \tag{2}$$

$$C_{fi}|_{i=\{1,2\}} = \frac{1}{\omega_p^2 (L_{fi})} \tag{3}$$

being $T_{nX}$ the value of the equivalent inductance of data transformer, and $n$-term adopts the values $T$ (for $T_{TX}$) and $R$ (for $T_{RX}$).

## III. ANALYTICAL STUDY OF TRANSFER FUNCTIONS

In this section, the transfer functions of SS and *LCC* compensation systems with power and data transfer are derived by including nonideality of the reactive components. The comparative gain and phase analysis is conducted also for the data
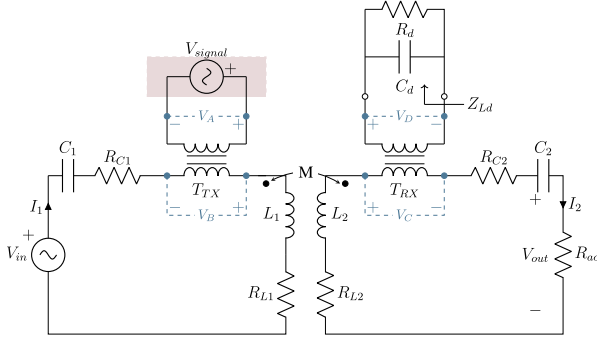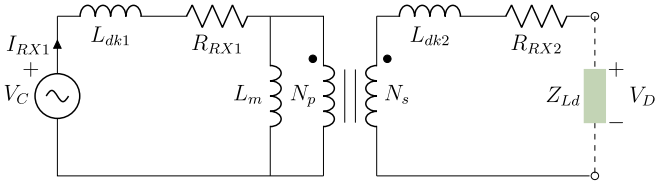
Fig. 4. SS power transfer equivalent scheme.



Fig. 5. TX transformer equivalent scheme.

channel, while the analyzes available in the literature miss some parasitic components and only refer to the power channel.

### A. SS Power Channel

The proposed scheme for the study of the power channel in an SS system is shown in Fig. 4 where $V_{\text{signal}}$ represents the data generator and $V_{\text{in}}$ the power source for the EV charge.

According to [19], a transformer equivalent scheme is that shown in Fig. 5, where $L_{dki}$, $R_{\text{RX}i}$, and $L_m$ are the leakage inductance, the winding resistance, and the magnetizing inductance, respectively. $Z_{Ld}$ is the transformer output equivalent impedance and $N_p$ and $N_s$ are the primary and secondary coil turns, whose values are used to calculate the turn ratio as

$$n_{\text{RX}} = \frac{N_p}{N_s} \tag{4}$$

$$Z_{Ld} = \frac{1}{\frac{1}{jX_{Cd}} + \frac{1}{R_d}} \tag{5}$$

$$L_{dki} = (1 - k)L_{di} \quad i=\{1,2\} \tag{6}$$

where $L_{di}$ is the self-inductance of the primary and secondary transformer windings.

According to Fig. 5, the primary and secondary impedances are $Z_p = R_{\text{RX}1} + jX_{Ldk_1}$ and $Z_s = R_{\text{RX}2} + jX_{Ldk_2}$, respectively. The impedance of the magnetization inductance is $Z_m = jX_{L_m}$.

To study the transformer impedance as reflected to the primary side, the equivalent impedance circuit is shown in Fig. 6.

The impedance reflected by the transformer is

$$Z_{\text{tfref}} = Z_p + \frac{n_{\text{RX}}^2 Z_m Z_s + Z_{Ld}}{Z_m + n_{\text{RX}}^2(Z_s + Z_{Ld})}. \tag{7}$$
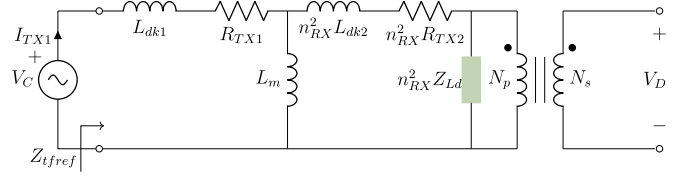


Fig. 6. TX transformer equivalent impedance.

The secondary circuit impedance is expressed as

$$Z_2 = jX_{L2} + R_{L2} + Z_{\text{tfref}} + jX_{C2} + R_{C2} + R_{\text{ac}} + R_2 \tag{8}$$

where $X_{L2}$ and $X_{\text{RX}}$ are power and data coil reactances, respectively, $R_2$ is the resistance of the connection wires, and $X_{C2}$ is the secondary capacitor reactance. The internal resistance of each element, such as $R_{L2}$, $R_{Ld}$, and $R_{C2}$ have to be considered. The equivalent load resistance after the rectification process of the battery resistance ($R_L$) is

$$R_{\text{ac}} = \frac{8}{\pi^2} R_L. \tag{9}$$

The primary circuit equivalent impedance is

$$Z_1 = jX_{L1} + R_{L1} + jX_{\text{TX}} + R_{\text{TX}} + jX_{C1} + R_{C1} + R_1. \tag{10}$$

Applying Kirchhoff's laws and simplifying terms, the gain, SS circuit power transfer function is derived as follows:

$$G_{p\text{SS}} = \left.\frac{V_{\text{out}}}{V_{\text{in}}}\right|_{V_{\text{signal}}=0} = \frac{j\omega M R_{\text{ac}}}{Z_1 Z_2 + (\omega M)^2}. \tag{11}$$

### B. SS Data Channel

The estimation of the transfer function for data transmission in an SS compensated system is carried out by means of the calculation of three partial transfer functions $G_{1\text{SS}}$, $G_{2\text{SS}}$, and $G_{3\text{SS}}$, being $G_{1\text{SS}} = \frac{V_B}{V_A}$, $G_{2\text{SS}} = \frac{V_C}{V_B}$, and $G_{3\text{SS}} = \frac{V_D}{V_C}$, as shown in Fig. 4.

To analyze the transfer function of the data channel, the transfer function governing the operation of a transformer must be studied, as this is the method by which the data signal is fed into the circuit. Thus, the transformer voltage transfer function for a nonideal transformer is

$$G_{3\text{SS}} = \frac{n_{\text{RX}} Z_{Ld} X_{L_m}}{n_{\text{RX}}^2 (Z_s + Z_{Ld})(Z_p + Z_m) + Z_p Z_m}. \tag{12}$$

The impedance of the power channel secondary circuit, considering the transformer equivalent impedance is

$$Z_{2d} = jX_{L2} + R_2 + jX_{C2} + Z_{\text{tfref}} + R_{\text{ac}} \tag{13}$$

$$Z_{1d} = jX_{L1} + R_{L1} + jX_{C1} + R_{C1} + R_1 \tag{14}$$

$$Z_{\text{refd}} = \frac{(\omega M)^2}{Z_{2d}}. \tag{15}$$

With the equivalent impedance of the secondary circuit and the equivalent impedance of the primary circuit, the partial transfer function can be determined as follows:

$$G_{2\text{SS}} = \frac{j\omega M Z_{\text{tfref}}}{Z_{1d} Z_{2d} + j\omega M^2}. \tag{16}$$
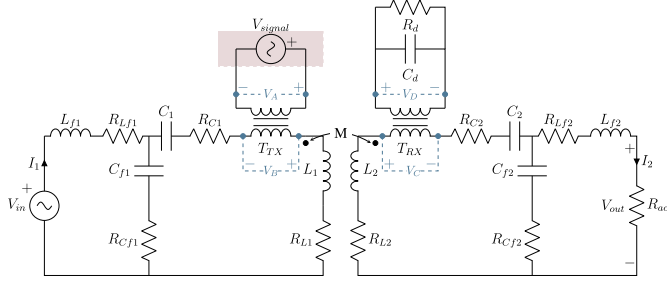
Fig. 7.  *LCC* power transfer equivalent scheme.

Finally, the transfer function resulting in the voltage gain of the data transformer is analyzed. For this, the same theoretical approach as in the (12) is used

$$Z_{LdTX} = Z_1 + Z_{refd}. \tag{17}$$

In this case, according to (17), the load impedance of the transmitting transformer is considered to be $Z_1$ together with the reflected impedance $Z_{refd}$, while the primary and secondary impedances of the transformer are

$$Z_{ptf} = jX_{Ldk1} + R_{LTX1} \tag{18}$$

$$Z_{stf} = jX_{Ldk2} + R_{LTX2} \tag{19}$$

and

$$n_{TX} = \frac{N_{TX1}}{N_{TX2}}. \tag{20}$$

Thus, the partial gain is determined as

$$G_{1SS} = \frac{n_{TX}Z_{LdTX}Z_m}{n_{TX}^2(Z_{stf} + Z_{LdTX})(Z_{ptf} + Z_m) + (Z_{ptf}Z_m)}. \tag{21}$$

Applying the principle of superposition, the total transfer function is derived as

$$G_{dataSS} = \left.\frac{V_D}{V_A}\right|_{V_{in}=0} = G_{1SS}G_{2SS}G_{3SS}. \tag{22}$$

## C. LCC Power Channel

In an *LCC* compensation system, an inductor and a capacitor, named $L_{fi}$ and $C_{fi}$, are added to the basic SS configuration. Fig. 7 shows an equivalent scheme of *LCC* circuit.

To determine the transfer function of an *LCC* circuit, some variables are defined as follows:

$$\alpha = X_{Lf1} + R_{Lf1} + X_{Cf1} + R_{Cf1} \tag{23}$$

$$\beta = X_{Cf1} + R_{Cf1} \tag{24}$$

$$\gamma = X_{L1} + R_{L1} + X_{C1} + R_{C1} + ZT_{TX} + X_{Cf1} + R_{Cf1} \tag{25}$$

$$\delta = -j\omega M \tag{26}$$

$$\epsilon = X_{L2} + R_{L2} + X_{C2} + R_{C2} + Z_{tfref} + X_{Cf2} + R_{Cf2} \tag{27}$$

$$\eta = X_{Cf2} + R_{Cf2} \tag{28}$$

$$\lambda = R_{ac} + X_{Lf2} + R_{Lf2} + X_{Cf2} + R_{Cf2}. \tag{29}$$

The relation between these variables is determined by Kirchhoff's voltage law (KVL) as

$$\begin{cases} \alpha I_1 - \beta I_p = V_{in} \\ -\beta I_1 + \gamma I_p - \delta I_s = 0 \\ -\delta I_p + \epsilon I_s - \eta I_2 = 0 \\ -\eta I_s + \lambda I_2 = 0. \end{cases} \tag{30}$$

Solving the system of equations and extracting the relation between $V_{in}$ and $V_{out}$, taking into account that $V_{out}$ is

$$V_{out} = I_2 R_{ac}. \tag{31}$$

The voltage gain in an *LCC* circuit is defined as

$$G_{pLCC} = \left.\frac{V_{out}}{V_{in}}\right|_{V_{signal}=0}$$

$$= \frac{\beta\delta\eta R_{ac}}{-\beta^2\eta^2 + \epsilon\lambda\beta^2 + \alpha\lambda\delta^2 + \alpha\gamma\eta^2 - \alpha\gamma\epsilon\lambda}. \tag{32}$$

## D. LCC Data Channel

The calculation of the total transfer function of the *LCC* system is carried out through the calculation of three partial gains, following the same criteria used for the SS topology. The analysis carried out to determine the partial gains $G_{1LCC}$ and $G_{3LCC}$ is the same as that performed for the determination of the gains $G_{1SS}$ and $G_{3SS}$, so the equation for $G_{3LCC}$ is equal to (12) and the equation for $G_{1LCC}$ is equal to (21).

The influence of the data receiving transformer on the power circuit is first analyzed to derive $G_{2LCC}$ expression. The reflected impedance of the receiver transformer follows (15). Thus, applying KVL, the following equations are considered:

$$\alpha_d = X_{Lf1} + R_{Lf1} + X_{Cf1} + R_{Cf1} \tag{33}$$

$$\beta_d = X_{Cf1} + R_{Cf1} \tag{34}$$

$$\gamma_d = X_{L1} + R_{L1} + X_{C1} + R_{C1} + R_1 + X_{Cf1} + R_{Cf1} \tag{35}$$

$$\delta_d = -j\omega M \tag{36}$$

$$\epsilon_d = Z_{tfref} + X_{L2} + R_{L2} + X_{C2} + R_{C2}$$
$$+ R_2 + X_{Cf2} + R_{Cf2} \tag{37}$$

$$\eta_d = X_{Cf2} + R_{Cf2} \tag{38}$$

$$\lambda_d = R_{ac} + X_{Lf2} + R_{Lf2} + X_{Cf2} + R_{Cf2}. \tag{39}$$

Therefore, the partial transfer function $G_{2LCC}$ for the *LCC* compensation system is

$$G_{2LCC} = \frac{\alpha_d\delta_d\lambda_d Z_{tfref}}{-\beta_d^2\eta_d^2 + \epsilon_d\lambda_d\beta_d^2 + \alpha_d\lambda_d\delta_d^2 + \alpha_d\gamma_d\eta_d^2 - \alpha_d\gamma_d\epsilon_d\lambda_d}. \tag{40}$$

The total gain is calculated as follows:

$$G_{dataLCC} = \left.\frac{V_D}{V_A}\right|_{V_{in}=0} = G_{1LCC}G_{2LCC}G_{3LCC}. \tag{41}$$

As an additional analysis, it should be mentioned that a study of the effect that the particular values of the *LCC* compensation
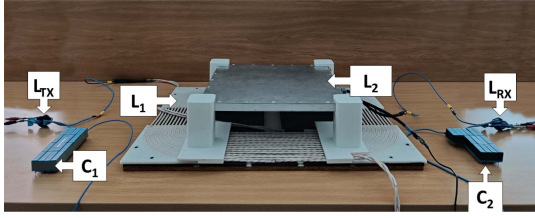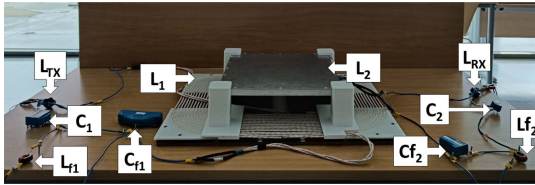
Fig. 8.   SS experimental implementation.



Fig. 9.   *LCC* experimental implementation.

system have on the data channel has been performed. Three different configurations have been analyzed for this study: the real case, with the compensation values indicated in this article, and two extra cases in which the value of $L_{f1}$ has been increased and decreased by 50%, recalculating the rest of the components with (2) and (3). This study shows that the values selected for the compensation system affect the shape of the curve in the kHz frequency range, keeping invariable the performance of the circuit in the MHz order. Thus, the conclusions related to the data transmission are valid for other configurations of the compensation systems.

## IV. EXPERIMENTAL EVALUATION

To experimentally validate the theoretical derivations, two different prototypes have been designed and tested: one with an SS compensation system and the other with an *LCC* compensation system. Here, elements common to both solutions have been used. An ITECH-BSS2000 power source, has been utilized to generate the input dc voltage; four CREE KIT8020-CRD-8FF1217P-J evaluation boards have been used as inverters and rectifiers, they include C2M0080120D CREE SiC MOSFETs. The inverter has been controlled by an algorithm developed for a PICKIT4 device, with a DSPIC30f4011 digital signal processor (DSP). Finally, EV battery is modeled with an EA-EL 9080-200 electronic load.

The prototype main coils ($L_1$ and $L_2$) are wound with an AWG-38 Litz wire and comply with SAE J2954. Both primary and secondary coils include ferromagnetic material to improve power transmission. The compensation systems capacitors and coils have the values previously calculated in Section I. In Figs. 8 and 9, the experimental implementation of these designs are shown.

The circuit for data transmission consists of two toroidal transformers with 3:3 and 3:4 transformer turn ratios for the transmitter and receiver circuits, respectively. To generate a 1 MHz signal, a GF-232 function generator has been used.



Fig. 10.   Power channel experimental magnitude and phase validation of (a) SS compensation system; (b) *LCC* compensation system.

The values of the used components, including the main coils and the mutual inductance, have been measured with a Wayne Kerr 4300 LCR meter at 85 kHz and 1 MHz.

As shown in Table II, the values differ from each other, so for the power channel the 85 kHz values have been used, while for the data channel, the values measured at 1 MHz have been selected. This criterion has been established since in the experimental tests, a signal of 85 kHz was transmitted for the power channel, while a 1 MHz carrier has been used for the data channel. The variation of the measurements is mainly caused by the different performance that the electrical components present under different frequencies. In fact, as can be observed, even in the same type of component this performance can be different due to factors such as material, geometry, dimensions, or core permeability.

To validate the power section transfer function, a frequency ranging from 20 to 400 kHz has been established. While, a frequency ranging from 150 to 2.5 MHz has been utilized to validate data channel derivations.

### A. Power Channel

The experiments for the power channel validation have been carried out under the conditions listed in Table III.

As can be seen in Fig. 10, no significant difference is observed between real system theoretical curves (with the par-

TABLE I
RELATED WORK

| Ref. | System transfer function | SS–LCC power channel comparative analysis | SS–LCC data channel comparative analysis | 3- axes misalignment analysis | Parasitic resistance consideration | Bandwidth analysis | Backward data transmission | Analysed parameters |
|---|---|---|---|---|---|---|---|---|
| [8] | ✓ | | | | | | ✓ | Gain, Efficiency, SNR |
| [9] | ✓ | | | | | | ✓ | Gain, Efficiency, SNR |
| [10] | ✓ | | | | | | | Gain |
| [11] | ✓ | | | | | | ✓ | Efficiency |
| [12] | ✓ | | | | | ✓ | ✓ | Gain, SNR |
| [13] | ✓ | | | | | | | Gain, SNR |
| [14] | ✓ | ✓ | | | | | | Gain, Efficiency |
| [15] | ✓ | ✓ | | | | | | Gain, Efficiency |
| [17] | | ✓ | | | | | | Efficiency |
| Proposal | ✓ | ✓ | ✓ | ✓ | ✓ | ✓ | ✓ | Gain, Efficiency, SNR, channel capacity |

TABLE II
MEASURED CIRCUITS PARAMETERS

| | Param. | Measured value at 85 kHz | Measured value at 1 MHz | Param. | Measured value at 85 kHz | Measured value at 1 MHz |
|---|---|---|---|---|---|---|
| SS | $L_1$ | 61.93 $\mu$H | 92.32 $\mu$H | $C_1$ | 55.84 nF | 74.49 nF |
| | $R_{L1}$ | 0.07 $\Omega$ | 0.30 $\Omega$ | $R_{C1}$ | 0.05 $\Omega$ | 0.10 $\Omega$ |
| | $L_2$ | 45.95 $\mu$H | 67.19 $\mu$H | $C_2$ | 81.36 nF | 126.62 nF |
| | $R_{L2}$ | 0.05 $\Omega$ | 2.86 $\Omega$ | $R_{C2}$ | 0.04 $\Omega$ | 0.08 $\Omega$ |
| LCC | $L_1$ | 61.93 $\mu$H | 92.32 $\mu$H | $L_{f1}$ | 18.27 $\mu$H | 18.05 $\mu$H |
| | $R_{L1}$ | 0.07 $\Omega$ | 0.30 $\Omega$ | $R_{Lf1}$ | 0.26 $\Omega$ | 4.23 $\Omega$ |
| | $L_2$ | 45.95 $\mu$H | 67.19 $\mu$H | $L_{f2}$ | 19.62 $\mu$H | 19.44 $\mu$H |
| | $R_{L2}$ | 0.05 $\Omega$ | 2.86 $\Omega$ | $R_{Lf2}$ | 0.15 $\Omega$ | 4.26 $\Omega$ |
| | $C_1$ | 75.46 nF | 98.38 nF | $C_{f1}$ | 190.60 nF | 177.04 nF |
| | $R_{C1}$ | 0.02 $\Omega$ | 0.05 $\Omega$ | $R_{Cf1}$ | 0.04 $\Omega$ | 0.07 $\Omega$ |
| | $C_2$ | 122.16 nF | 114.33 nF | $C_{f2}$ | 181.12 nF | 154.58 nF |
| | $R_{C2}$ | 0.01 $\Omega$ | 0.02 $\Omega$ | $R_{Cf2}$ | 0.05 $\Omega$ | 0.03 $\Omega$ |
| DATA | $L_{TX1}$ | 5.75 $\mu$H | 3.87 $\mu$H | $L_{RX1}$ | 5.84 $\mu$H | 3.91 $\mu$H |
| | $R_{LTX1}$ | 0.87 $\Omega$ | 4.68 $\Omega$ | $R_{LRX1}$ | 0.91 $\Omega$ | 4.85 $\Omega$ |
| | $L_{TX2}$ | 5.84 $\mu$H | 3.99 $\mu$H | $L_{RX2}$ | 10.18 $\mu$H | 6.75 $\mu$H |
| | $R_{LTX2}$ | 0.87 $\Omega$ | 4.65 | $R_{LRX2}$ | 1.61 $\Omega$ | 8.58 $\Omega$ |
| | $C_{TX}$ | 4.02 nF | 4.03 nF | $C_{RX}$ | 4.02 nF | 4.03 nF |

TABLE III
POWER TRANSMISSION PARAMETERS

| Topology | $V_{in}$ (V) | $P_{in}$ (W) | $V_{out}$ (V) | $P_{out}$ (W) | Eff. (%) |
|---|---|---|---|---|---|
| SS | 80 | 1096.80 | 173.30 | 1048.98 | 95.64 |
| *LCC* | 100 | 1062 | 166.40 | 967.28 | 91.08 |

asitic resistances), and the experimental results, so that the validity of the equations proposed can be verified. It should be noted that the ideal curves (without considering the parasitic resistances) are not included in this figure. The reason is that in case of power channel, with a working frequency of 85 kHz, the components resistances are negligible, so the difference between the curves is imperceptible. The curves obtained for the power channel in each of the configurations are largely different. In the case of the SS configuration, the curve shows an increasing trend until it reaches a maximum at about 85 kHz, and then continues to decrease as the frequency increases. The *LCC* configuration has the following three peaks: one at about 55 kHz, one at about 85 kHz, and a final peak at 115 kHz.
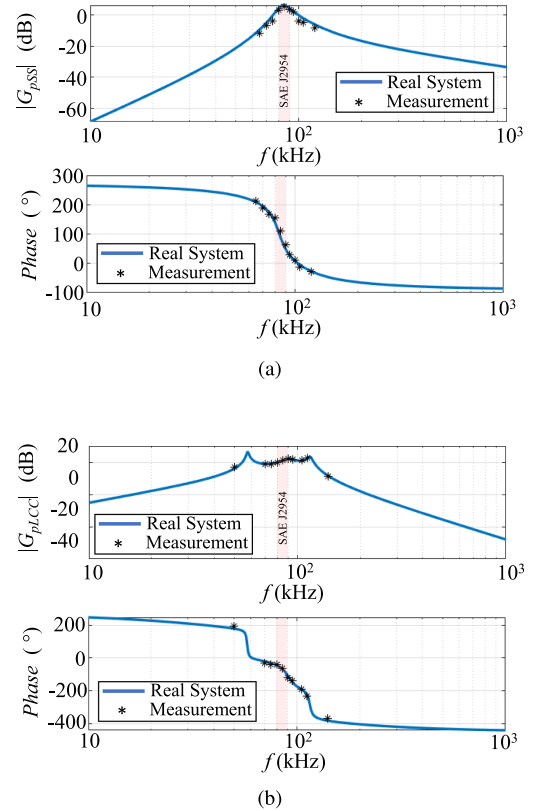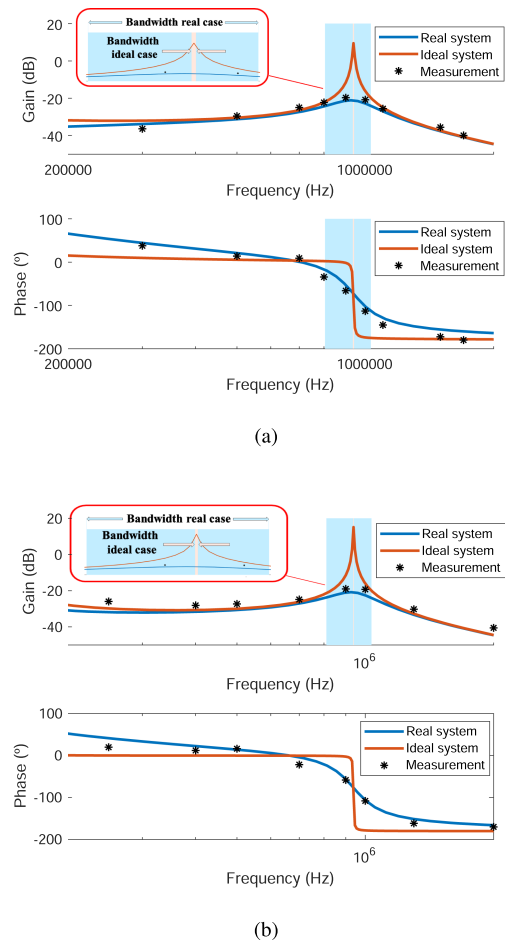


Fig. 11. Data channel experimental magnitude and phase validation of (a) SS compensation system; (b) *LCC* compensation system.

The SS configuration results in a 6.61 dB gain at 85 kHz, while the *LCC* gain only reaches 4.95 dB.

### B. Data Channel

The results of the data channel transfer function are shown in Fig. 11. This figure shows that the error between theoretical and experimental values is negligible. Moreover, both plots have the

same trend, as well as experimental values, that is, the theoretical curves fit the experimental ones. The plots also show that there are no significant bandwidth differences in the 1 MHz frequency range.

In the range close to 1 MHz, the behavior of both systems is similar. In the case of the *LCC* compensation system, the gain at the 1 MHz frequency is slightly higher than the SS system ($-20.5$ dB compared to $-22$ dB, which is equivalent to 0.11 against 0.07 V/V).

The trend of the curves from about 500 kHz onwards is similar. However, at lower frequencies, the *LCC* compensation system has an increasing trend up to about 100 kHz, while the SS compensation system has a decreasing trend, as shown in Fig. 11.

The same figure shows that the parasitic resistances of the components must be considered in the analysis to achieve a more accurate model.

In SS system, the ideal magnitude gain is 9.48 dB, while in *LCC* system this value is 18.40 dB. The magnitude gain error found between the ideal system and the real model with parasitic components is 32.48 and 37.2 dB. As can be seen, this difference between the two cases is very significant. For this reason, an analytical study has been carried out to deduce, which are the components that most contribute to this difference. This study first analyzed the effect of the parasitic resistances of the components of the power circuit ($R_{Ci}$ and $R_{Li}$ for SS, and $R_{Ci}$, $R_{Li}$, $RC_{fi}$, $R_{Lfi}$ for *LCC*). The results of this first analysis have determined that these parasitic resistances mainly affect the kHz frequency range, close to the resonance frequency of the power circuit. Therefore, these elements do not have a direct effect on the significant differences found in the MHz frequency order. In a second analysis, the effect of the data circuit components ($R_{LTX1}$, $R_{LTX2}$, $R_{LRX1}$, and $R_{LRX2}$) has been studied. In this case, it is found that the component that causes this difference in gain between the ideal circuit and the real circuit is the parasitic resistance of the data injection/extraction transformer. To perform this study, an analysis of both compensation systems has been carried out considering five different resistances values of $R_{LTX1}$, $R_{LTX2}$, $R_{LRX1}$, and $R_{LRX2}$. These values range from the ideal case, where the resistance values of the data transformers are $0\,\Omega$, to the real case, with the values presented in Table II. The result of this study confirms that as the value of these resistors increases, the gain at a frequency close to 1 MHz decreases considerably, thus justifying the significant differences found in Fig. 11. The value of this $R_{LTXi}$ and $R_{LRXi}$ depends on many variables, such as core geometry, size, and material used. It is recommended that this value be as low as possible at 1 MHz to maximize the maximum gain of the system at that frequency.

The BW is also significantly affected, as in the ideal case the values are reduced from 228 967 to 6 kHz for SS and from 224 387 to 3.5 kHz for *LCC*. This difference in bandwidth is due to the fact that for the ideal case, the curve narrows considerably at its highest point. Considering that bandwidth is calculated as the difference between the frequency points that are 3 dB below the maximum value, the narrowing of the curve causes the bandwidth value to reduce sharply.
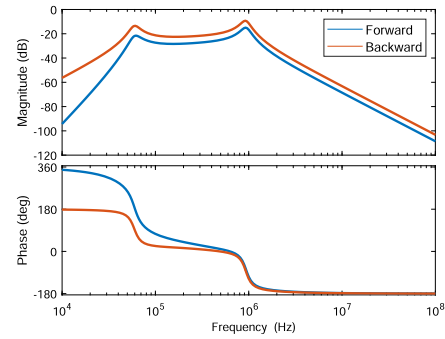


Fig. 12. SS forward and backward communication transfer functions.

As for the phase analysis, similar results have been observed for both configurations in this frequency range demonstrating through experimental tests the validity of the proposed theoretical analysis.

It should be mentioned that the curves for the data channel transfer functions have been compared with different solutions described in the related work for SS [20], [21] and for *LCC–LCC* [13], [22]. The results show that the trend of the curves is similar for each topology, being the differences caused by the particular values of the power circuit components. Therefore, this analysis can be extrapolated to other systems with components of different values.

To complete the previous analysis, it is carried out a comparative study of the performance of the SS and *LCC* topologies depending on the direction of data transmission.

It is of interest to verify if there is any change in this transfer function if the data transmission is in the opposite direction. It must be highlighted that the backward data transmission is commonly used in control techniques as V2G services, where the communication is necessary from the secondary to the primary circuit. To do this analysis, two different cases are studied. In the first case, it is considered the isolated data channel with a single voltage source. In the second case, the simultaneity of two voltage sources (for power and data transmission) will be considered in the calculation and comparison of the transfer function.

After performing these two analyzes, it is found that in the case of the isolated data channel, the transfer function remains constant regardless of the direction of data transmission. This is fulfilled for both the SS and the *LCC* compensation system.

However, the analysis conducted for the two simultaneous sources gives different results, as can be seen in Figs. 12 and 13. In SS compensation system, it can be observed that in backward transmission the values of the gain are higher over the entire frequency range. At frequencies close to 1 MHz, the difference is up to 5.7 dB, while at the 85 kHz power frequency this difference is 8.17 dB, with an increasing trend of this variation as the frequency decreases. Similarly, the phase also shows variations, which are more significant at frequencies below 100 kHz. In the case of *LCC*, variations are only found in the power frequency range with variations up to 8.66 dB, however, for frequencies close to data transmission (1 MHz) the differences
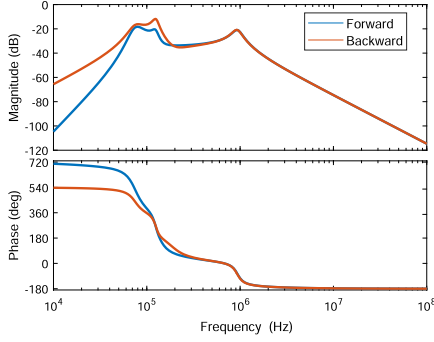
Fig. 13.    *LCC* forward and backward communication transfer functions.

do not exceed 0.2 dB. Therefore, the SS compensation system shows an asymmetric performance when the direction of data transmission changes, while the *LCC* remains constant in that frequency range.

## V. MISALIGNMENT ANALYSIS

The transmitting and the receiving coils are often not perfectly aligned in a practical charging process of an EV.

According to the SAE J2954 standard, the used system complies with the WPT2/Z1 configuration as the gap between the primary and secondary coil is established at 105 mm. To test the performance of the system, three different types of conditions are established: vertical, horizontal, and angular variations, as shown in Fig. 14. For the vertical variation ($Z$-axis), a maximum distance of 60 mm from the original position is established, since, in accordance with SAE J2954, this maximum variation is specified by the manufacturer. On the other hand, a maximum 80 mm distance along the $Y$-axis is considered, so that is compliant with the limits established by the standards ($\pm100$ mm). Finally, a maximum deviation of $10°$ has been considered for the angular variation.

The trend of transfer function curves in misalignment conditions, with the experimental validation, is shown in Fig. 15. The model used for these curves is the real model (with parasitic resistances), so that it is comparable with the experimental results measured in the laboratory.

The results of the misalignment study are shown in Table IV, where the theoretical and experimental values are compared. The variation of the coupling coefficient in that range does not make a significant difference in bandwidth for both the configurations. In the SS system, a maximum 5.061 kHz variation occurs in the bandwidth for the vertical axis, while for the horizontal and angular cases, the maximum variations are 1.799 and 3.668 kHz, respectively. The *LCC* configuration results in lower differences as follows: a maximum 2.476 kHz variation for $Z$-axis and 0.990 kHz and 1.288 kHz for horizontal and angular misalignment, respectively, have been measured. These results show that: a) the most significant differences in both configurations are in the case of $Z$-axis misalignment; b) the SS system has twice the value found in *LCC* system. The most relevant gain variations are also found in the vertical misalignment for both SS and *LCC*, with a gain drop of $-6.6$ dB (equivalent to $-0.46$ V/V). Finally,

## TABLE IV
### THEORETICAL VERSUS EXPERIMENTAL RESULTS WITH MISALIGNMENT

|  | Misalignment | Condition | $k$ | BWtheo (kHz) | BWexp (kHz) |
|---|---|---|---|---|---|
|  |  | 105 mm | 0.26 | 228.97 | 228.00 |
|  | Vertical | 135 mm | 0.20 | 226.08 | 222.00 |
|  |  | 165 mm | 0.16 | 223.91 | 217.00 |
|  |  | 0 mm | 0.26 | 228.97 | 228.00 |
| SS | Horizontal | 4 mm | 0.26 | 228.41 | 225.00 |
|  |  | 8 mm | 0.25 | 227.17 | 222.00 |
|  |  | $0°$ | 0.26 | 228.97 | 228.00 |
|  | Angular | $6°$ | 0.24 | 227.33 | 227.00 |
|  |  | $10°$ | 0.21 | 225.23 | 224.00 |
|  |  | 105 mm | 0.26 | 224.39 | 226.00 |
|  | Vertical | 135 mm | 0.20 | 223.01 | 225.00 |
|  |  | 165 mm | 0.16 | 221.91 | 223.00 |
|  |  | 0 mm | 0.26 | 224.39 | 226.00 |
| *LCC* | Horizontal | 4 mm | 0.26 | 224.19 | 223.00 |
|  |  | 8 mm | 0.25 | 223.40 | 221.00 |
|  |  | $0°$ | 0.26 | 226.39 | 226.00 |
|  | Angular | $6°$ | 0.24 | 223.44 | 221.00 |
|  |  | $10°$ | 0.21 | 223.09 | 219.00 |

this study shows that the phase remains practically unchanged in both configurations.

## VI. INTERFERENCE ANALYSIS

An analysis of the effect of power channel in data transmission, and vice-versa, is performed in this section. First, it is necessary to compute the effect that the coexistence of the two voltage sources have on the system. To do so, the final value of the output voltage must be computed.

In the calculation of an electrical circuit with two independent voltage sources, superposition principle is applied. The output voltage can be expressed as $V_{\text{out}} = V_{\text{out1}} + V_{\text{out2}}$, being $V_{\text{out1}}$ and $V_{\text{out2}}$ the output voltages when considering only one of the voltage sources activated. Thus, these terms can be related to the input voltages as $V_{\text{out1}} = G_{\text{power}}V_{\text{in}}$ and $V_{\text{out2}} = G_{\text{data}}V_{\text{signal}}$, being $V_{\text{in}}$ the input voltage of the power source, and $V_{\text{signal}}$ the input voltage of the data source, following the nomenclature used throughout this article. The values of $G_{\text{power}}$ and $G_{\text{data}}$ are the transfer functions of both single-input single-output (SISO) systems. Thus, the relation between both transfer functions and the output voltage is

$$V_{\text{out}} = G_{\text{power}}V_{\text{in}} + G_{\text{data}}V_{\text{signal}}. \quad (42)$$

The SISO transfer functions of the isolated power and data channels are those indicated in Section III, achieving as a result (11) and (22) for SS, and (32) and (41) for *LCC*. It should be noted that both in SS and *LCC*, the power transfer function is calculated over $R_{\text{ac}}$. However, to analyze the effect of the simultaneity of both voltage sources, these transfer functions should be computed over the equivalent impedance of data transformer $Z_{\text{tfref}}$. Thus, the new values for the power channel transfer functions for both topologies are

$$G_{\text{power}_{d\text{SS}}} = \frac{j\omega M Z_{\text{tfref}}}{Z_1 Z_2 + (\omega M)^2} \quad (43)$$

$$G_{\text{power}_{d\text{LCC}}} = \frac{\beta\delta\lambda Z_{\text{tfref}}}{-\beta^2\eta^2 + \epsilon\lambda\beta^2 + \alpha\lambda\delta^2 + \alpha\gamma\eta^2 - \alpha\gamma\epsilon\lambda}. \quad (44)$$

Finally, by substituting in (42) $G_{\text{power}}$ by the new power transfer functions calculated, as well as replacing $G_{\text{data}}$ by the data
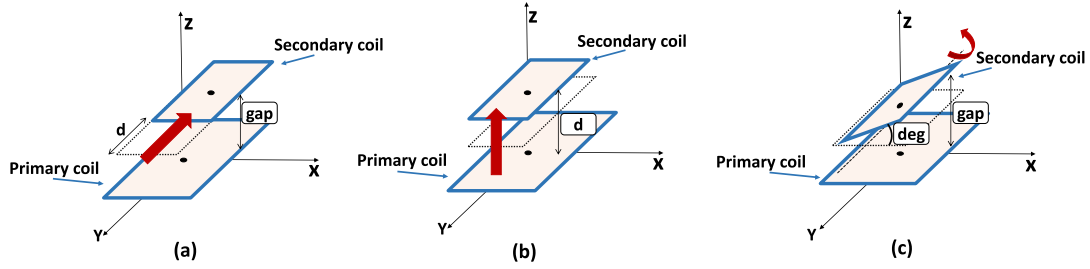
Fig. 14.    Misalignment conditions. (a) Horizontal. (b) vertical. (c) Angular.
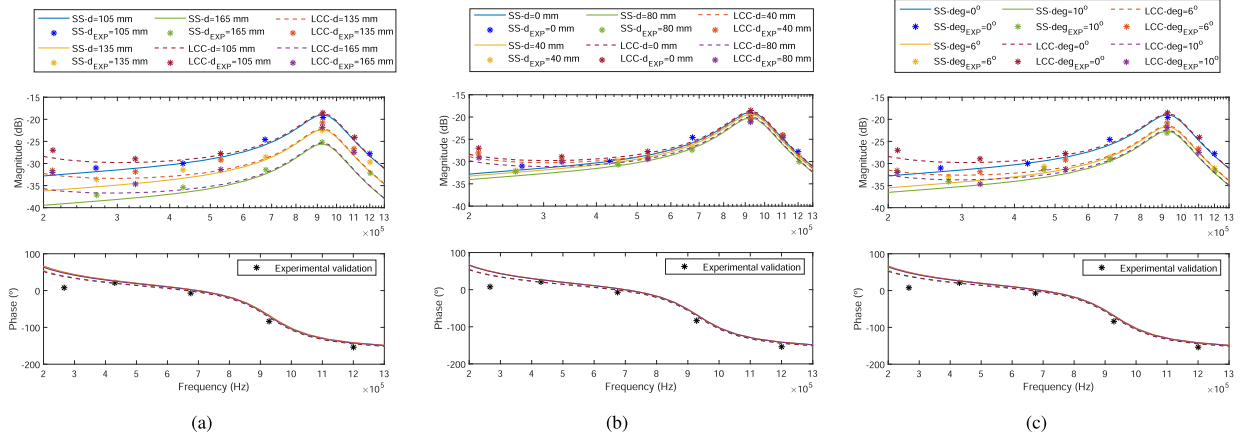


Fig. 15.    SS and *LCC* misalignment analysis. (a) Vertical. (b) Horizontal. (c) Angular.

channel transfer functions of each compensation system, the output voltage is given by

$$V_{\text{outSS}} = G_{\text{power}_{dSS}} G_{3SS} V_{\text{in}} + G_{\text{dataSS}} V_{\text{signal}} \qquad (45)$$

$$V_{\text{outLCC}} = G_{\text{power}_{dLCC}} G_{3LCC} V_{\text{in}} + G_{\text{dataLCC}} V_{\text{signal}}. \qquad (46)$$

This final equation allows us to estimate the effect of both voltage sources in the circuit. It should be mentioned that in case of $G_{\text{power}} V_{\text{in}}$ term, $G_{3SS}$ and $G_{3LCC}$ should be also considered, as the gain calculation is performed over the output resistor of the receiver transformer ($R_d$), so this final stage transfer function is needed.

In order to analyze the interference between the data and the power transmission signals, an analysis of the SNR variable will be carried out in this section. For this purpose, simultaneous transmission of power and data has been carried out, as shown in Fig. 16. In this figure, VL1 is the voltage measured in the primary inductor ($L_1$) and VRX is the voltage measured in the primary side of the reception data transformer ($T_{\text{RX}}$).

The expression used for SNR calculation is SNR = $20\log_{10}(\frac{V_{\text{signal}}}{V_{\text{noise}}})$, where $V_{\text{signal}}$ and $V_{\text{noise}}$ are the voltage value of the data signal and the voltage value of the power signal, respectively. Both values have been measured in the output resistor ($R_d$) of the data circuit.

Furthermore, it is interesting to include an analysis of the channel capacity for each topology. Following the Shannon–Hartley theorem, the value of the channel capacity is given by $C = B\log_2(1 + \frac{V_{\text{signal}}}{V_{\text{noise}}})$, being $B$ the bandwidth of data communication in Hz.
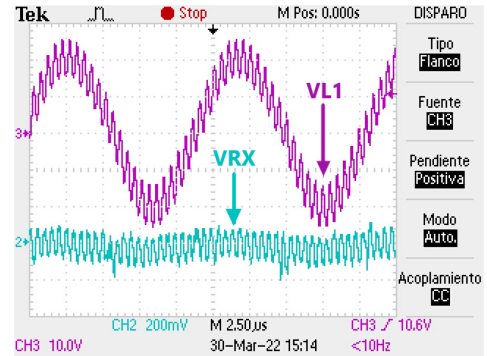


Fig. 16.    Simultaneous transmission of power and data-waveforms.

The SNR and capacity analyzes are carried out for different input voltage values of the power signal (from 10 to 60 V), as well as for each of the misalignment distances presented in Section V. In Table V, the results obtained for the case $V_{\text{in}} = 60$ V, as an example, are shown.

From Fig. 17, it can be deduced that, for both topologies, the SNR value decreases as the input voltage value of the power signal increases. However, although this behavior is common to both topologies, it can be observed that the SS system has higher SNR and capacity values than the *LCC* system. The reason for this difference lies in the performance of the circuit in the presence of two simultaneous voltage sources (data and power transmission source). In the SS compensation system, the coexistence of two simultaneous sources results in an increase of the gain in the transfer function of the system over its entire

TABLE V
SNR AND CAPACITY ANALYSIS IN MISALIGNMENT CONDITIONS FOR $V_{\text{IN}} = 60$ V

| | | SS | | LCC | |
|---|---|---|---|---|---|
| | | BW (Hz) | Capacity (bits/s) | BW (Hz) | Capacity (bits/s) |
| Vertical | $d = 105$ mm | 224 822 | 132 629.99 | 221 071 | 36 394.87 |
| | $d = 135$ mm | 222 398 | 126 546.10 | 220 117 | 30 124.18 |
| | $d = 165$ mm | 221 681 | 124 242.98 | 218 655 | 25 212.26 |
| Horizontal | $d = 0$ mm | 224 822 | 132 629.99 | 221 071 | 36 394.87 |
| | $d = 40$ mm | 224 269 | 131 407.32 | 220 148 | 35 001.58 |
| | $d = 80$ mm | 223 657 | 129 567.62 | 219 915 | 34 008.98 |
| Angular | deg $= 0°$ | 224 822 | 132 629.99 | 221 071 | 36 394.87 |
| | deg $= 6°$ | 223 493 | 127 641.72 | 219 917 | 31 172.55 |
| | deg $= 10°$ | 222 506 | 126 595.51 | 219 350 | 29 822.00 |
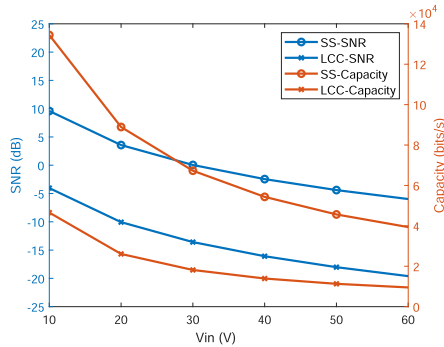


Fig. 17.  SNR and Capacity comparison SS and *LCC* topologies.

frequency range. In contrast, in the *LCC* topology, this gain increase is only observed at frequencies close to the kHz range. Therefore, in *LCC* compensation, the gain increases for the frequency of the power signal, while it remains constant for the data signal.

This performance leads to two main conclusions. The first one is that in this type of SWPDT circuits, SS compensation has better results in terms of SNR, since with the simultaneity of the two voltage sources, the gain increases for all frequencies. However, this first conclusion allows us to draw a second deduction, which is the fact that the *LCC* topology has no variation depending on the direction of data transmission. In the *LCC* transfer function of the circuit with two simultaneous sources, the curve remains unchanged at frequencies of the order of MHz. This means that this system is invariable when new inputs are added to the circuit. Having a consistent and invariable data transmission system can result in more robust and reliable communication during the charging process. In addition, this advantage can be useful for systems where there is a bidirectional communication between primary and secondary circuit, but this communication is performed in different time slots (half-duplex). In this case, the data carrier signal can be the same for both directions. The invariability of *LCC* topology can lead to the implementation of the same data circuit both for forward and backward communication.

## VII. Conclusion

In this article, a theoretical and experimental study of both SS and *LCC–LCC* configurations, which are the most widely used in SWPDT systems, has been conducted. Experimental tests validated the proposed theoretical derivations, which have

been developed by considering all the parasitic resistances of the components constituting the systems. The analysis developed in this article has demonstrated the importance of considering all these parasitic resistances, since they have a direct effect on the data channel. In the experimental validations, the efficiency values obtained are higher than 90 % in both cases.

In addition, a theoretical analysis of the system under different misalignment conditions has been carried out. The conditions have been defined according to the SAE J2954. The two config-uration power channel transfer functions greatly differ in both magnitude and phase. For the data channel, both the phase and magnitude differences are less significant, especially at frequencies around 1 MHz. From the misalignment analysis, it is concluded that the bandwidth variation does not have a significant difference in both SS or *LCC*. The higher variation occurs in SS compensation system, for vertical misalignment, with a variation of 5.061 kHz between 105 and 165 mm. For the *LCC* configuration, the most remarkable value has also been found in the *Z*-axis with a value of 2.476 kHz, however, the BW differences correspond to approximately half of the SS value. In terms of gain and phase, no significant variations can be highlighted between both configurations.

With respect to the SNR analysis, it can be concluded that both the SS and *LCC* configurations show a decreasing trend as the input voltage of the power signal increases. The SS configuration shows higher values of SNR than the *LCC* configuration. This is due to the transfer functions of both circuits when considering two simultaneous sources. In the case of SS, the inclusion of the source for power transmission means an increase in gain over the whole frequency range, while for *LCC* this increase only occurs in the range close to the power frequency. This makes the data circuit in the *LCC* configuration invariable to new inputs in the circuit, as it remains unchanged.

Finally, it is noteworthy that the performance of the circuit in backward data transmission is different in each topology. In SS compensation, backward transmission results in a curve with higher gain for all frequencies. On the other hand, the *LCC* circuit keeps the gain curve unchanged for the backward transmission case. From this, it can be concluded that although the gain is higher in SS topology, the *LCC* configuration is more suitable for a symmetrical design of the SWPDT system.

## References

[1] F. Wen, X. Chu, Q. Li, and W. Gu, "Compensation parameters optimization of wireless power transfer for electric vehicles," *Electronics*, vol. 9, no. 5, 2020, Art. no. 789.

[2] M. Venkatesan et al., "A review of compensation topologies and control techniques of bidirectional wireless power transfer systems for electric vehicle applications," *Energies*, vol. 15, no. 20, 2022, Art. no. 7816.

[3] J. Sallán, Juan L. Villa, A. Llombart, and J. F. Sanz, "Optimal design of ICPT systems applied to electric vehicle battery charge," *IEEE Trans. Ind. Electron.*, vol. 56, no. 6, pp. 2140–2149, Jun. 2009.

[4] Y. Yao et al., "Analysis and design of a simultaneous wireless power and data transfer system featuring high data rate and signal-to-noise ratio," *IEEE Trans. Ind. Electron.*, vol. 68, no. 11, pp. 10761–10771, Nov. 2021.

[5] X. Li, C. Tang, X. Dai, P. Deng, and Y. Su, "An inductive and capacitive combined parallel transmission of power and data for wireless power trans-fer systems," *IEEE Trans. Power Electron.*, vol. 33, no. 6, pp. 4980–4991, Jun. 2018.

[6] I. Casaucao, A. Triviño, and Z. Lin, "Simultaneous wireless power and data transfer for electric vehicle charging: A review," *IEEE Trans. Transport. Electrific.*, to be published, doi: 10.1109/TTE.2023.3309505.

[7] F. Corti, A. Reatti, M. C. Piccirilli, F. Grasso, L. Paolucci, and M. K. Kazimierczuk, "Simultaneous wireless power and data transfer: Overview and application to electric vehicles," in *Proc. IEEE Int. Symp. Circuits Syst.*, 2020, pp. 1–5.

[8] Y. Jing, W. Feng, K. Qiao, L. Yang, S. Wang, and L. Lu, "Simultaneous wireless power and data transfer system with full-duplex mode based on LCC/CLC resonant network," *IEEE Trans. Power Electron.*, vol. 38, no. 4, pp. 5549–5560, Apr. 2023.

[9] P. Wang, Y. Sun, Y. Feng, T. Feng, Y. Fan, and X. Li, "An improvement of SNR for simultaneous wireless power and data transfer system with full-duplex communication mode," *IEEE Trans. Power Electron.*, vol. 37, no. 2, pp. 2413–2424, Feb. 2022.

[10] J. Wu et al., "A simultaneous wireless information and power transfer system with independent channel for information transfer," *IEEE Access*, vol. 8, pp. 125610–125619, 2020.

[11] Y. Sun et al., "Bidirectional simultaneous wireless information and power transfer via sharing inductive link and single switch in the secondary side," *IEEE Access*, vol. 8, pp. 184187–184198, 2020.

[12] Y. Yao, H. Cheng, Y. Wang, J. Mai, K. Lu, and D. Xu, "An FDM-based simultaneous wireless power and data transfer system functioning with high-rate full-duplex communication," *IEEE Trans. Ind. Informat.*, vol. 16, no. 10, pp. 6370–6381, Oct. 2020.

[13] P. Y. Wang, L. Sang, and K. Wang, "Optimization of simultaneous wireless power and data transmission system with single coil," in *Proc. 8th Int. Conf. Power Electron. Syst. Appl.*, 2020, pp. 1–6.

[14] Y. Chen, H. Zhang, C.-S. Shin, K.-H. Seo, S.-J. Park, and D.-H. Kim, "A comparative study of S-S and LCC-S compensation topology of inductive power transfer systems for EV chargers," in *Proc. IEEE 10th Int. Symp. Power Electron. Distrib. Gener. Syst.*, 2019, pp. 99–104.

[15] W. Li, H. Zhao, J. Deng, S. Li, and C. C. Mi, "Comparison study on SS and double-sided LCC compensation topologies for EV/PHEV wireless chargers," *IEEE Trans. Veh. Technol.*, vol. 65, no. 6, pp. 4429–4439, Jun. 2016.

[16] A. Triviño-Cabrera, Z. Lin, and J. A. Aguado, "Impact of coil misalignment in data transmission over the inductive link of an EV wireless charger," *Energies*, vol. 11, no. 3, 2018, Art. no. 538.

[17] Y. Zhu, H. Wu, F. Li, Y. Zhu, Y. Pei, and W. Liu, "A comparative analysis of S-S and LCCL-S compensation for wireless power transfer with a wide range load variation," *Electronics*, vol. 11, no. 3, 2022, Art. no. 420.

[18] X. Liu, L. Clare, X. Yuan, C. Wang, and J. Liu, "A design method for making an LCC compensation two-coil wireless power transfer system more energy efficient than an SS counterpart," *Energies*, vol. 10, no. 9, 2017, Art. no. 1346.

[19] A. Ayachit and M. K. Kazimierczuk, "Transfer functions of a transformer at different values of coupling coefficient," *IET Circuits, Devices Syst.*, vol. 10, no. 4, pp. 337–348, 2016.

[20] Z. Qian, R. Yan, J. Wu, and X. He, "Construction and analysis of communication channels for simultaneous wireless power and data transmission," in *Proc. IEEE 44th Annu. Conf. Ind. Electron. Soc.*, 2018, pp. 4793–4798.

[21] Y. Wang, Y. Yao, Y. Guan, X. Liu, M. Liu, and D. Xu, "A novel modulation and demodulation method for wireless power and data transmission," in *Proc. IEEE Transp. Electrific. Conf. Expo, Asia-Pacific*, 2017, pp. 1–6.

[22] Y. Fan, Y. Sun, X. Dai, Z. Zuo, and A. You, "Simultaneous wireless power transfer and full-duplex communication with a single coupling interface," *IEEE Trans. Power Electron.*, vol. 36, no. 6, pp. 6313–6322, Jun. 2021.

**Inmaculada Casaucao** was born in Córdoba, Spain. She received the B.S. degree in electronics engineering and the master's degree in electronic systems for intelligent environments from the University of Málaga, Málaga, Spain, in 2019 and 2020, respectively. She is currently working toward the Ph.D. degree, which focuses on the simultaneous transmission of power and data in wireless chargers for electric vehicles, in the Mechatronics Engineering Programme from the University of Málaga, Málaga, Spain.

She has also worked on research projects related to microgrid design and control techniques for wireless bidirectional chargers.

**Alicia Triviño** received the master's degree in telecommunication engineering and in computer science engineering from the University of Málaga, Málaga, Spain, in 2002 and 2008, respectively.

She is currently an Associate Professor with the University of Málaga. In the field of electric vehicle wireless chargers, she has played an active role in designing and developing several prototypes, including features, such as bidirectionality and dynamic charging. Her thesis, which she defended in 2007, focused on wireless networks. Her research focuses on wireless power transfer.
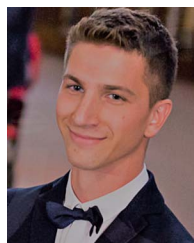
**Fabio Corti** (Member, IEEE) received the M.S. degree in electrical and automation engineering and the Ph.D. degree in industrial engineering from the University of Florence, Florence, Italy, in 2016 and 2019, respectively.

He was a Postdoctoral Research Fellow with Consiglio Nazionale delle Ricerche, Florence, Italy, in 2020. From 2020 to 2022, he was a Postdoctoral Research Fellow with the University of Perugia, Perugia, Italy. He is currently an Assistant Professor with the University of Florence. His research interests include modeling and control of dc–dc PWM and resonant converters wireless power transfer, energy storage characterization, and electric vehicle powertrain.

**Alberto Reatti** (Member, IEEE) received the M.S. degree in electronics engineering from the University of Florence, Florence, Italy, in 1988 and the Ph.D. degree in electrical engineering from the University of Bologna, Bologna, Italy, in 1993.

In 1992, he was an Associate Researcher with the Department of Electrical Engineering, Wright State University, Dayton, OH, USA. He has been an Associate Professor with the Department of Information Engineering, University of Florence, since 2000. He is responsible for agreements of cultural and scientific cooperation with the Department of Information Engineering and the Head of the Patent and Technology Transfer Board, University of Florence. He has authored or coauthored more than 110 papers. He holds two patents. His current research interests include high-frequency, resonant, and pulsewidth modulated dc–dc power converters; dc–ac inverters; modeling and control of converters; high-frequency magnetic devices; renewable power sources; energy saving; wireless power transfer; and investigations on reliability of switching power converters.

Dr. Reatti was the Chairperson for the Power Electronic and Power Systems Committee of the IEEE CAS Society.